Journal of Molecular Liquids 347 (2022) 118350

Contents lists available at ScienceDirect

Journal of Molecular Liquids

journal homepage: www.elsevier.com/locate/molliq

Structural specificity of groove binding mechanism between imidazolium-based ionic liquids and DNA revealed by synchrotron-UV Resonance Raman spectroscopy and molecular dynamics simulations

Fatemeh Fadaei [a,b], Mariagrazia Tortora [c,d], Alessandro Gessini [d], Claudio Masciovecchio [d], Sara Catalini [e], Jacopo Vigna [f], Ines Mancini [f], Andrea Mele [g], Jan Vacek [h], David Reha [a], Babak Minofar [a,*], Barbara Rossi [d,*]

[a] Laboratory of Structural Biology and Bioinformatics, Institute of Microbiology of the Czech Academy of Sciences, Zámek 136, Nové Hrady, Czech Republic
[b] Faculty of Science, University of South Bohemia in České Budějovice, Branišovská 1645/31A, 37005 České Budějovice, Czech Republic
[c] AREA SCIENCE PARK, Padriciano, 99, 34149 Trieste, Italy
[d] Elettra-Sincrotrone Trieste, S.S. 114 km 163.5, Basovizza, 34149 Trieste, Italy
[e] European Laboratory for Non-Linear Spectroscopy, LENS, Via Nello Carrara, 1, 50019, Sesto Fiorentino, Firenze, Italy
[f] Laboratory of Bioorganic Chemistry, Department of Physics, University of Trento, Via Sommarive, 14 - 38123 Povo Trento, Italy
[g] Department of Chemistry, Materials and Chemical Engineering "G. Natta", Politecnico di Milano, Piazza L. da Vinci 32, 20133 Milano, Italy
[h] Department of Medical Chemistry and Biochemistry, Faculty of Medicine and Dentistry, Palacky University, Hnevotinska 3, 775 15 Olomouc, Czech Republic

ARTICLE INFO

Article history:
Received 5 August 2021
Revised 18 November 2021
Accepted 14 December 2021
Available online 20 December 2021

Keywords:
Synchrotron UV Resonance Raman
Molecular dynamics
Ionic liquids
Nucleic acids
Solvation

ABSTRACT

The predicted capability of Ionic Liquids (ILs) in stabilizing the native structure of nucleic acids is relevant in biotechnology, especially for DNA storage and handling. In the present work, we implement a joint combination of advanced spectroscopic techniques such as synchrotron radiation-UV Resonance Raman spectroscopy (SR-UVRR) and molecular dynamics (MD) simulations for deepening insight into the sequence and structural specificity of the binding interactions between imidazolium-based ILs and both the phosphate groups and nucleobases in the minor and major grooves of double-stranded DNA. A 30-base pair double-stranded DNA structure has been chosen as a model of natural DNA. The experimental and simulation results give evidence of the predominance of a groove binding mechanism between ILs cations and DNA, with preferential interactions among guanine residues and the shorter alkyl-chain length on imidazolium cations. Raman experiments allowed us to detect both cooperative transition and reversible pre-melting structural transformations that involve specific tracts in the structure of DNA and are turned on at lower temperatures for guanine residues than for adenine ones. The more marked effect on the pre-melting states of adenine operated by the imidazolium-based ILs with chloride as anion suggests a selective strong interaction of this anion with the DNA's adenine-rich tracts. MD simulation results reveal the influence of ILs on the structural properties of DNA and provide more details about the solvation, interaction, stability and flexibility of DNA in the hydrated ILs. According to MD analyses, simultaneous electrostatic and hydrophobic interactions drive the shorter alkyl-chain length of imidazolium cations to have greater interplays with the DNA major groove.

1. Introduction

Thanks to the well-known programmability of the Watson-Crick pairing interactions, Deoxyribonucleic acid (DNA) is gaining a crucial role as the building block for developing innovative devices in nanotechnology and biomedical technology [1–4]. For instance, the sequence-based recognition mechanism of DNA has been employed in DNA micro-arrays of gene expression analyses [5] and in chips for gene sequencing by hybridization [6,7]. Nanoscale self-assembly methods have been used for constructing 2D

Abbreviations: ILs, Ionic Liquids; SR-UVRR, Synchrotron radiation-UV Resonance Raman spectroscopy; MD, Molecular dynamics; DNA, Deoxyribonucleic acid; UVRR, UV Resonance Raman; dsDNA, double-stranded DNA; [MIM]Cl, 1-methylimidazolium chloride; [EMIM]Cl, 1-ethyl-3-methylimidazolium chloride; [BMIM]Cl, 1-butyl-3-methylimidazolium chloride; [BMIM]Br, 1-butyl-3-methylimidazolium bromide; GAFF, General Amber Force Field; NVT, (constant number volume temperature); NPT, (constant number pressure temperature); LINCS, linear constraint solver; VMD, Visual Molecular Dynamics; RDF, Radial distribution function; RMSD, Root mean square deviation.

* Corresponding authors.
E-mail addresses: minofar@nh.cas.cz (B. Minofar), barbara.rossi@elettra.eu (B. Rossi).

https://doi.org/10.1016/j.molliq.2021.118350
0167-7322/

and 3D ordered structures of DNA [8] and design hybrid materials such as metallic nanoparticles [9]. However, the lack of suitable media in which nucleic acids can preserve their structures for a long time and under various conditions represents the obstacle for further applications of DNA in nanotechnology. Although DNA is considered reasonably stable in aqueous solutions, the degradation of its structure has been observed for extended storage periods at room temperature [10]. DNA is vulnerable to hydrolytic and oxidative damage in water [11,12]. Besides, non-physiological temperature, extreme pH and ionic strength or repeated freeze–thaw cycles can destroy the DNA helix structure and cause denaturation. Using aqueous DNA samples makes some technological processes in nanotechnology difficult since small volumes of water vaporize immediately under open-air conditions or at high temperatures [13]. For these reasons, finding appropriate media that ensure the long-lasting stability of DNA and help to overcome the limitations of aqueous buffers remains a challenging task.

Ionic liquids (ILs) are a class of organic salts almost liquid at room temperature that offer unique opportunities as alternative solvents or co-solvents in various physical and chemical conditions [14]. In the last two decades, ILs have gained increasing popularity in biotechnology for a broad range of applications. Both experimental and simulation works have addressed the potential benefits exerted by the neat or aqueous solutions of ILs in the stabilization and functioning of proteins and DNA [15–19]. Compared to more common co-solutes or co-solvents, the large number of anion/cation combinations of ILs offers the possibility to design tailor-made compounds for specific purposes. Moreover, certain remarkable features of ILs, such as their vanishing vapor pressure, provide an attractive alternative to water in a large variety of applications [20]. Unlike the multiple studies reported on the effects of ILs on the structure and function of proteins, much less is known about the properties of DNA dissolved in pure or aqueous solution of ILs [13,19,21–23]. The pioneering study of MacFarlane [24] provided the first experimental observations that DNA preserves its structure in various ILs during long-term storage at room temperature. A joint molecular dynamics simulation and spectroscopic study [25] suggest that site-specific interactions of IL cations and anions with DNA favor the long-term structural stability of nucleic acids in aqueous solutions of ILs. Other studies reveal that several types of ILs contribute to enhance DNA stability without modifying its structure [26–33]. ILs can be employed for controlling the properties of the nucleic acids, like increasing the sensitivity of electrochemical DNA sensors [34] and developing more efficient protocols for DNA extraction and purification [35]. Finally, an increasing number of studies regarding applications of ILs for the delivery of nucleic acids into the eukaryotic cells have emerged in more recent years [23].

The potential use of ILs as new-generation solvents and/or co-solvents for DNA deserves a further understanding of the molecular origin of the observed enhanced stability of nucleic acids in ionic liquids. In this context, it is important to account that even small differences in ionic composition of ILs can drastically change the effect on DNA properties. Several studies point out that ILs with imidazolium-based cations are efficient co-solvents of water in improving the structural stability of DNA [25,27,28,31–33,36]. This effect arises from specific interactions of the cation and anion with the minor and major grooves of nucleic acids. However, there is no complete agreement on the driving forces that dominate this interaction mechanism between imidazolium-based ILs and DNA. For some authors [25,27,28,31,33], the dominant factors that lead to an increasing stabilization and preservation of DNA structure in ILs aqueous solutions are associated with i) the DNA groove binding with IL cations through hydrophobic and polar forces and ii) the partial dehydration of DNA operated by ILs. An alternative view proposes the semi-intercalation binding mode of the imidazolium cation with DNA, revealing also that this interaction becomes stronger as the alkyl chain length on the imidazolium ring increases [32]. Another interpretation suggests that the most important contribution to the stability of DNA structure has to be ascribed to the ability of anions in imidazolium-based ILs to establish a greater number of hydrogen bonds with the nucleobases of DNA than the cations [26]. Overall, the investigations mentioned above evidence the need to rationalize the interaction properties of ILs components, i.e. cations and anions, with nucleic acids to predict the efficacies of aqueous solutions of ILs for DNA solvation and stabilization.

In the present work, we implement a joint combination of advanced spectroscopic techniques such as synchrotron radiation-UV Resonance Raman spectroscopy (SR-UVRR) and molecular dynamics (MD) simulations for investigating structure-specific interactions between imidazolium-based ILs and a 30-base pair double-stranded DNA structure. Preliminary experimental studies performed on large nucleic acid molecules dissolved in ILs/water solutions [37–40] addressed the type and the strength of network interactions established between ILs and DNA molecules, suggesting a possible mechanism of cation- and anion- mediated structural stabilization of nucleic acids. Further, the thermal stability of DNA has been found to increase as a function of the concentration of 1-butyl-3-methylimidazolium chloride [BMIM]Cl [38]. The present study aims to clarify the sequence and structural specificity of the interactions (electrostatic, hydrophobic, hydrogen bonds) between the ILs and phosphate groups and nucleobases in the DNA minor and major grooves, besides addressing the formation of modified nucleic acid structures in hydrated ILs. Multi-wavelength UV Resonance Raman (UVRR) spectroscopy enables the measurement of experimental quantities directly related to pair hydrogen bond strength and base stacking forces in nucleic acid strands [37–39,41,42]. The fine tuning of the excitation wavelength achievable by synchrotron radiation (SR) source provides the UVRR technique selectivity for local and global DNA conformational changes. This allows monitoring local events such as base conformational changes or to probe intermediate structural states involving dangling ends of DNA sequence that are more exposed to the interaction with cations and anions of ILs [37–39]. In this study, molecular dynamics simulations carried out on the same double-stranded DNA structure support and further develop the experimental outcomes from SR-UVRR spectroscopy. DNA structure along the simulation trajectories is analyzed here in the presence of ILs and compared with its crystal B-form to investigate the structure and the groove dimensions of DNA. Finally, we have studied the binding pattern of ILs to DNA.

2. Materials and methods

2.1. Chemicals and sample preparation

Both fully complementary oligonucleotides (sequence of strand 1 [ss1]: AAC CCA GAT GTC CTA CAG GAT AGC TCG CAG; 53 % of GC pairs, without 5-phosphate termination, 9184.94 Da) were synthesized by the company VBC Genomics (Vienna, Austria). The double-stranded DNA (dsDNA) was prepared to 100 μM duplex concentration in Tris buffer 10 mM at pH 7.4, heated for 5 min at 90 °C and slowly cooled down to room temperature. The formation of the double-stranded structure has been checked through circular dichroism (CD) measurements using a spectropolarimeter JASCO J-810. The CD spectrum recorded on a 10 μM sample of dsDNA is shown in Fig. S1(a). The characteristic CD profile of double-stranded DNA comprising a positive and a negative band at about 270 and 245 nm, respectively, is clearly distinguishable. In addition to spectrophotometric methods, native gel electrophoresis was

used to confirm the formation of duplex DNA as shown in Fig. S1 (b). The electrophoretic mobility of dsDNA was in accordance with molecular marker (M). Both DNA single strands (ssDNA) migrated faster compared to ds version depending on their MW. In this way, dsDNA duplex formation had been checked for each sample used in this study. There is also clear evidence that ds and ss-DNA samples did not undergone aggregation or fragmentation under experimental conditions used. The ionic liquids 1-methylimidazolium chloride [MIM]Cl, 1-ethyl-3-methylimidazolium chloride [EMIM]Cl, 1-butyl-3-methylimidazolium chloride [BMIM]Cl and 1-butyl-3-methylimidazolium bromide [BMIM]Br (see Fig. S2(a) for chemical structures of IL) were acquired from IoLiTec with a purity of 99%. For the main purpose of this work, the procedure of water removal was not critical. However, in order to know the starting water content of ILs before the dilution, all the ILs have been dried inside a desiccator under vacuum with phosphorus pentoxide for 48 h at room temperature. After the treatment, the water content of all the ILs was ca. 100 ppm (Karl Fischer), which we assumed to be a reasonable level in view of further dilutions. For preparing dsDNA/ILs samples, each IL has been added to the solution of dsDNA at 100 μM and diluted with Tris buffer solution 10 mM at pH 7.4 to reach the final concentration of 54 mM of IL and 10 μM of dsDNA, corresponding to about 177 molecules of IL for each base-pair of DNA. This concentration of ILs has been chosen on the basis of previous Raman investigations carried out on large DNA molecules [38] that evidenced a stabilization effect exerted by methylimidazolium-based IL on DNA starting from about 80 molecules of IL for each base pair. Moreover, at the specified buffer concentration of 10 mM, the contribution of the added ILs to the overall ionic strength makes acceptable the approximation of considering all the measurements of DNA in pure Tris buffer and in Tris/ILs solutions carried out under the comparable conditions of ionic strength. All the solutions were freshly prepared for UVRR measurements and they appeared limpid before the running of experiments and after the thermal heating.

2.2. UVRR measurements and analysis of spectra

UVRR spectra were collected by exploiting the synchrotron-based UVRR set-up available at the BL10.2-IUVS beamline of Elettra Sincrotrone Trieste (Italy) [43]. All DNA and DNA/IL solutions were measured in the temperature range between 291 and 375 K using 250 and 266 nm as exciting wavelengths. The 250 nm wavelength was set by regulating the undulator gap and using a Czerny-Turner monochromator (Acton SP2750, Princeton Instruments, Acton, MA, USA) equipped with a holographic grating with 1800 groves/mm for monochromatizing the incoming synchrotron radiation. The excitation wavelength at 266 nm was provided by a CryLas FQSS 266-Q2, Diode Pumped Passively Q196 Switched Solid State Laser. Raman signal was collected in back-scattered geometry, analyzed by using a single pass of a Czerny-Turner spectrometer (Trivista 557, Princeton Instruments, 750 mm of focal length) equipped with holographic grating at 1800 g/mm and detected using a CCD camera. The calibration of the spectrometer was standardized using cyclohexane (spectroscopic grade, Sigma Aldrich). The final radiation power on the samples was kept at about 40 and 200 μW for excitation with 250 and 266 nm, respectively. Any possible photo-damage effect due to a prolonged exposure of the sample to UV radiation was avoided by continuously spinning the sample cell during the measurements. The comparison between the individual spectra acquired repeatedly for each sample showed no gradual changes to the spectra with respect to accumulation number, ensuring that any sample photodegradation due to UV radiation was observed.

For each set of temperature-dependent measurements, the UVRR spectra of the DNA samples have been collected at every temperature without moving the cell and by maintaining the same focus of the excitation radiation on the sample. In these conditions, we can assume that the scattering volume is practically the same for each measurement. Therefore, the temperature-dependent UVRR spectra obtained for each DNA sample do not need further normalization. The difference spectra have been computed by subtracting the UVRR spectrum measured at the lowest temperature (291 K) from each spectrum recorded at the selected higher temperatures. For each Raman spectrum, after subtraction of a flat baseline, the central wavenumber position of the peaks of interest has been estimated by fitting the spectra with a suitable number of Gaussian functions. We have assessed the intensity of the bands of interest through an integration algorithm applied to the wavenumber region of interest. Standard error bars in the plots have been estimated through the suitable routines of Origin Pro 2021 software.

2.3. UV–VIS measurements

UV/VIS absorption spectra were collected with a Perkin Elmer LAMBDA™ 25 UV/VIS spectrometer operating in double-beam mode and equipped with plug-n-play single cell Peltier with stirrer for the temperature control. UV/VIS spectra were recorded on the samples of dsDNA (1 μM in Tris buffer) and dsDNA 1 μM with addition of ILs at the final concentration of 5.3 mM in Tris buffer in the temperature range between 293 and 373 K with $\Delta T = 5$ K. All solutions were freshly prepared in a rectangular quartz cell of 10 mm path-length. The UV spectra were recorded in the range from 200 to 700 nm at a scanning speed of 480 nm/min and 1 nm of bandwidth.

2.4. Molecular dynamics simulations

For performing the MD simulations and quantifying the interaction of DNA with the ILs ([MIM]Cl, [EMIM]Cl, [BMIM]Cl, [BMIM]Br) in the aqueous solutions, the General Amber Force Field (GAFF) [44] was used for DNA and the imidazolium-based ILs. It is worthy to mention that the general accuracy of GAFF in the case of ILs solvents was tested and GAFF has been widely used in IL simulations for years. For example, Sprenger and his coworkers [45] examined the accuracy of the generic AMBER force field for the case of ionic liquids. In their study, thermodynamic and transport parameters of a collection of 19 room-temperature ionic liquids were calculated using molecular dynamics and compared to the experiment. According to the results, GAFF can reproduce these properties with good accuracy when compared to experiment and with similar accuracy when compared to other published force fields. In another study, Picalek et al [46] did the molecular dynamics investigation of the interfacial structure of aqueous solutions of 1-butyl-3-methylimidazolium tetrafluoroborate. Both nonpolarizable and polarizable force fields for aqueous solutions of ILs were used to explain the anomalous dependence of the surface tension on concentration. The general GAFF parameter set was used to provide a good description of the surface properties of the pure IL. In addition, Jiang et al. [47] did MD simulations using both electronically nonpolarizable and polarizable models to analyze 1-hydroxyethyl-4-amino-1,2,4-triazolium nitrate (HEATN). The GAFF was used for the nonpolarizable model. Their findings revealed a link between molecular structure, dynamics, and other physical properties for this class of IL, which matched the experimental results. In this work, a total number of 67 molecules of cations and 67 molecules of anions were added randomly to reach the desired IL concentrations (54 mM) in a cubic box with dimension 12.7 × 12.7 × 12.7 nm, where the box later solvated by water molecules. Packmol package was used for random distribution of the salts in the simulation boxes [48,49].

Since the salts and water molecules were added to the simulation box at random, certain undesirable interactions might arise in the systems, necessitating minimization. In this study, the steepest descent minimization approach was utilized to eliminate all unfavorable interactions. After minimization, all systems were equilibrated by performing 100 ps NVT (canonical ensemble) restrained simulations followed by 100 ps NPT (isothermal–isobaric ensemble). Equilibration proceeded with the production runs where the linear constraint solver (LINCS) algorithm [50] was employed for all bonds involving hydrogen atoms and short range non-bonded interactions were cut off by 1.2 nm. Long-range electrostatic interactions were treated by the particle mesh Ewald method [51] procedure. For the production of initial velocities, Maxwell–Boltzmann distribution was used for all simulations. V-rescale coupling algorithm was used [52] with the coupling constant of 0.1 ps to ensure constant temperature and pressure during the simulations. MD production runs were performed in NPT ensemble for 100 ns at 300 K where 2 fs time step was used. Data for further analysis were stored in every 5 ps for all simulations. Gromacs 2018 program package was used for performing MD simulations [53–57]. Also, for visualizations and preparation of snapshots [58], Visual Molecular Dynamics (VMD) was used. After the simulation, some strategies including radial distribution function (RDF) and root mean square deviation (RMSD) [59] were done to extract relevant information about the system. In details, the RDF is used to describe the distribution of solvent molecules around one specific molecule or atom. Also, the RMSD is computed to show the deviations of the backbone atoms of dsDNA from its initial structure and represents how structures and parts of structures alter over time as compared to the starting point.

3. Results and discussion

Non-resonance Raman spectra of nucleic acids are limited by the strong overlap of the different bases' ring modes so that the individual bands cannot be clearly resolved. The selective excitation of Raman spectra at different UV-wavelengths offers the advantage to distinguish most the bands of interest for the individual bases in nucleic acids, thanks to the enhancement patterns observed at the different excitations [60,61]. As shown in previous works [37,39], a comparison of the 266 and 250 nm-excited spectra of DNA can conveniently isolate the adenine dA and guanine dG contributions, respectively.

3.1. Local and cooperative structural transitions of guanine residues in hydrated ILs

The enhancement factors [37,60] show that the ring vibrations of guanine are the dominant contributions in the UVRR spectra recorded with 250 nm as excitation wavelength. Fig. 1(a)-(b) displays the temperature behavior of UVRR spectra, collected using 250 nm as excitation wavelength, for dsDNA in Tris buffer with the absence and presence of [EMIM]Cl, as an example. The panels visualize the evolution of the difference spectra obtained by subtracting the spectrum measured at the lowest temperature from the Raman profiles measured at the indicated temperatures (intermediate traces in Fig. 1(a)-(b)). UVRR spectra of dsDNA in Tris buffer and in [EMIM]Cl/Tris at 291 and 375 K are reported at the bottom and the top of Fig. 1. At the excitation wavelength of 250 nm, Raman spectra of DNA are dominated by the vibrational signals arising from guanine dG bases [37,38,41,60,61], such as the prominent modes dGI $\sim$ 1483 cm^{-1} and dGII $\sim$ 1582 cm^{-1} labeled in Fig. 1(a). Both these signals are sensitive structural markers of base stacking interactions and hydrogen bonds (H-bonds) involving the guanine residues [62–64]. This is mainly due to the strong in-plane character of these vibrational modes that are attributed to the N7 = C8 and C8-N9 ring stretching coupled with C8-H in-plane deformation of the dG purine group (dGI mode) [60,62,65,66] and to the N3-C4, C4=C5 and C5-N7 stretching motions of the same purine moiety (dGII mode) [63,65,67] (for the numbering of atoms of nucleobases see Fig. S2(b)). The Raman signals arising from purine residues of DNA include the broad band at $\sim$ 1332 cm^{-1} (Fig. 1(a)) that results from the overlap between base ring vibrations assigned to adenine dA and guanine dG residues [62,66].

The UVRR spectra reported in Fig. 1(b) illustrate that the main Raman bands assigned to dsDNA are also detectable in the sample of DNA dissolved in an aqueous solution of IL, with a minor spectral contribution from the Raman signals of the ionic liquid.

In the wavenumber region 1200–1800 cm^{-1}, many perturbations are observed in the 250 nm-excited UVRR spectra of dsDNA in Tris and in [EMIM]Cl/Tris as the temperature is raised, in terms of change in intensity and frequency of the main Raman bands (Fig. 1). This is well evidenced by the temperature trend observed for the Raman difference spectra, which reveals a remarkable increase in the intensity of the Raman bands at $\sim$ 1332, 1483 and 1582 cm^{-1} as a function of temperature. The intensity recovery of the mode dGI $\sim$ 1483 cm^{-1} (Raman hyperchromic effect) is mainly associated with i) the H-bonds breaking and base unstacking and to ii) local structural changes, such as reversible rupture or weakening of H-bonds as well as bases tilting that specifically involve the guanine residues in the structure of DNA [37,64–66,68–71]. The thermal pathway for the dGI Raman band of dsDNA is reported in Fig. 2 and records i) a reversible increase in intensity at low temperature (i.e. the peak observed at $\sim$ 299 K) and ii) a sharp transition detected at higher temperature (about 330 K, inflection point of the curves).

The latter sudden increase of the resonance Raman band dGI finds correspondence in the marked hyperchromicity detected in the UV absorbance melting curve of dsDNA at the temperature of $\sim$ 327 K (Fig. S3). Since the increase of optical density of DNA is connected with the disturbance of stacking interactions between bases, the marked increment of dGI band intensity may reflect the cooperative structural perturbation of guanine bases associated with the helix to coil transition (melting) of dsDNA promoted by the increment of temperature [37–39,41,63,64,69,70]. The dG structural transition probably entails a progressive partial disruption of guanine stacking supported by the increment of temperature. The disappearance of Raman hyperchromicity of the dGI band of dsDNA at high temperatures (Fig. 2) indicates that no further changes in the DNA secondary structure involving guanine residues are detected in this temperature region [69]. The semi-quantitative analysis of melting profiles reported in Fig. 2 allows the determination of quantitative descriptors of the thermal stability of dsDNA in absence and presence of ILs. In the temperature region above 310–320 K, the trend observed for the Raman band dGI exhibits a sudden jump that resembles a cooperative transition. A simple sigmoidal function $I(T)$ can satisfactorily fit such a two-state melting profile, as suggested in previous Raman investigations on DNA [42,72], given by:

$$I(T) = \frac{A + B exp\left(\frac{\Delta H_G}{R}\left(\frac{1}{T_{G_{coop}}} - \frac{1}{T}\right)\right)}{1 + exp\left(\frac{\Delta H_G}{R}\left(\frac{1}{T_{G_{coop}}} - \frac{1}{T}\right)\right)} \quad (1)$$

where A and B define the lower and upper limit of ordinate (Raman spectral band intensity), R is the gas constant and ΔH_G and $T_{G_{coop}}$ are the enthalpy variation and the transition temperature associated with the structural process involving dG bases. The mid-transition temperature $T_{G_{coop}}$ corresponds to the temperature at which the fraction of single-stranded molecules in the sample of DNA is equal

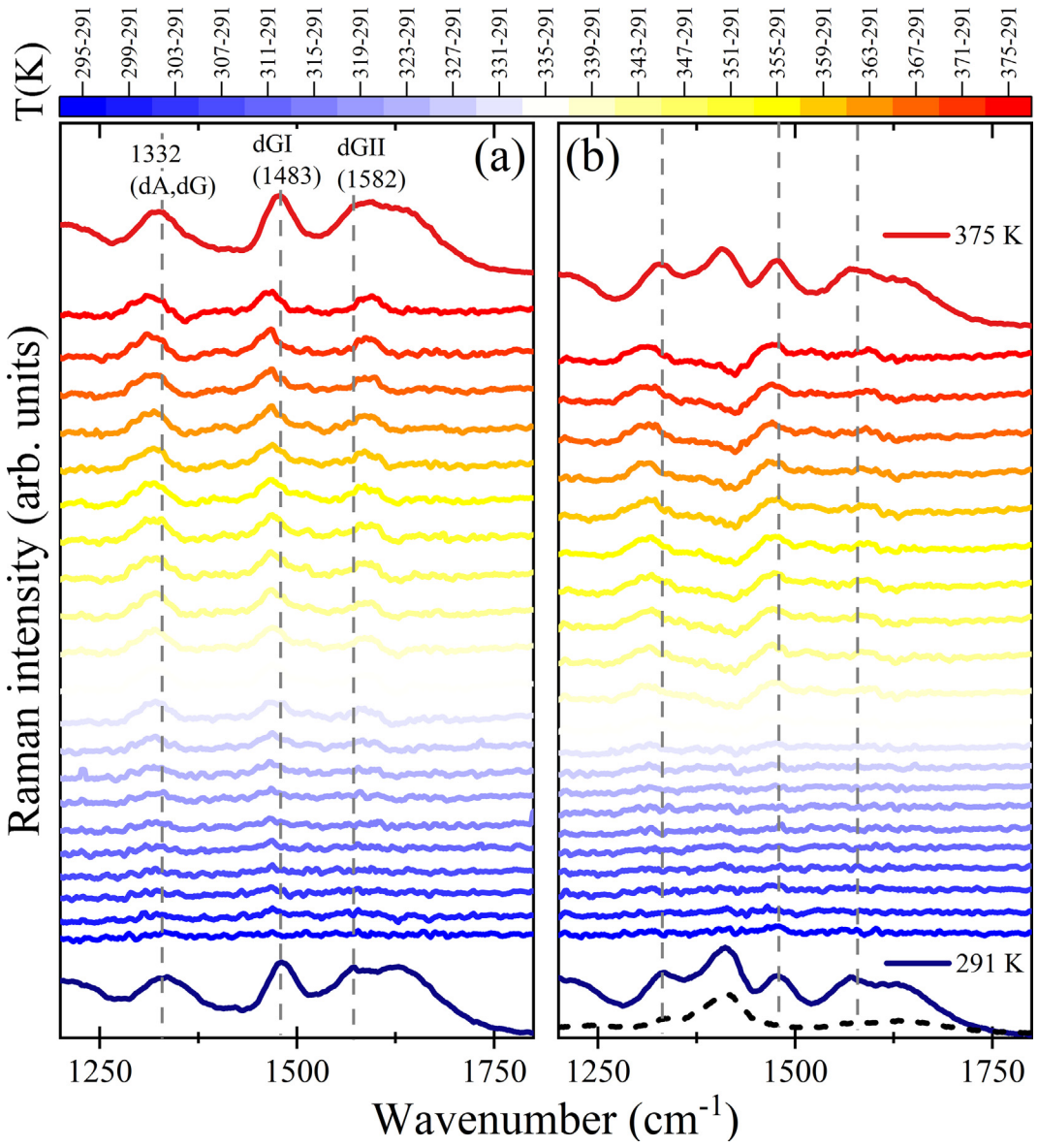

Fig. 1. 250 nm-excited Raman spectra of dsDNA (10 μM) in Tris buffer (a) and dsDNA in [EMIM]Cl/Tris (b) collected at 291 K (bottom trace) and 375 K (top trace); intermediate traces are the difference spectra computed by subtracting the spectrum measured at the lowest temperature from the spectrum at the indicated temperatures. The spectrum of [EMIM]Cl/Tris solution is also reported (dashed line in panel b).

to that of double-stranded species. It is usually obtained by analyzing oligonucleotide melting curves generated by different spectroscopic methods through well-described equations [73,74]. The fitting of Raman data of Fig. 2 with Eq. (1) constitutes a convenient method for estimating, with a relative good precision, the values of the cooperative dG transition temperature $T_{G_{coop}}$ for dsDNA in absence and presence of various imidazolium-based ILs (see values reported in Table 1). Figs. S4 and S5 in SI show that the values obtained for $T_{G_{coop}}$ by using the fitting procedure mentioned above are equivalent to those estimated through the Raman data analysis method proposed in the ref. [73,74].

The thermal paths of Fig. 2 and the $T_{G_{coop}}$ data of Table 1 reveal the different effects of ionic liquids on the thermally activated structural changes localized on guanine bases of dsDNA, as evidenced by the higher $T_{G_{coop}}$ transition temperature for dsDNA with [EMIM]Cl and [MIM]Cl. The formation of a preferential interaction between the cations of imidazolium-based ILs and the guanine residues on DNA grooves probably affecting the double helix thermal structure stability can explain this finding [25,27,28,31,33]. This is also consistent with the significant number of H-bonds that were found to exist between the oxygen and nitrogen of guanine and oxygen of thymine as acceptors and the activated C-H bonds of the imidazolium ring as donors [25]. Conversely, the similar temperature dependence of the dGI band observed for dsDNA in buffer and in [BMIM]Cl/Tris and [BMIM]Br/Tris suggests a comparable reduction in the extent of base stacking interactions along all the stages of the melting transition for these ILs.

It has to be remarked that the UV Raman intensity of the dGI band detects cooperative structural changes that are specifically localized on guanine-pairs during the dsDNA melting [37,38,41]. This is evident by considering the $T_{G_{coop}}$ values and the melting transition temperatures T_m calculated by UV absorbance experiments and reported in Table 1. Only a slight increment of the melting temperature (about 1.5 K) is observed for dsDNA dissolved in [EMIM]Cl/Tris solution in comparison with Tris buffer, while the corresponding variation of $T_{G_{coop}}$ is about 4 K for the same system

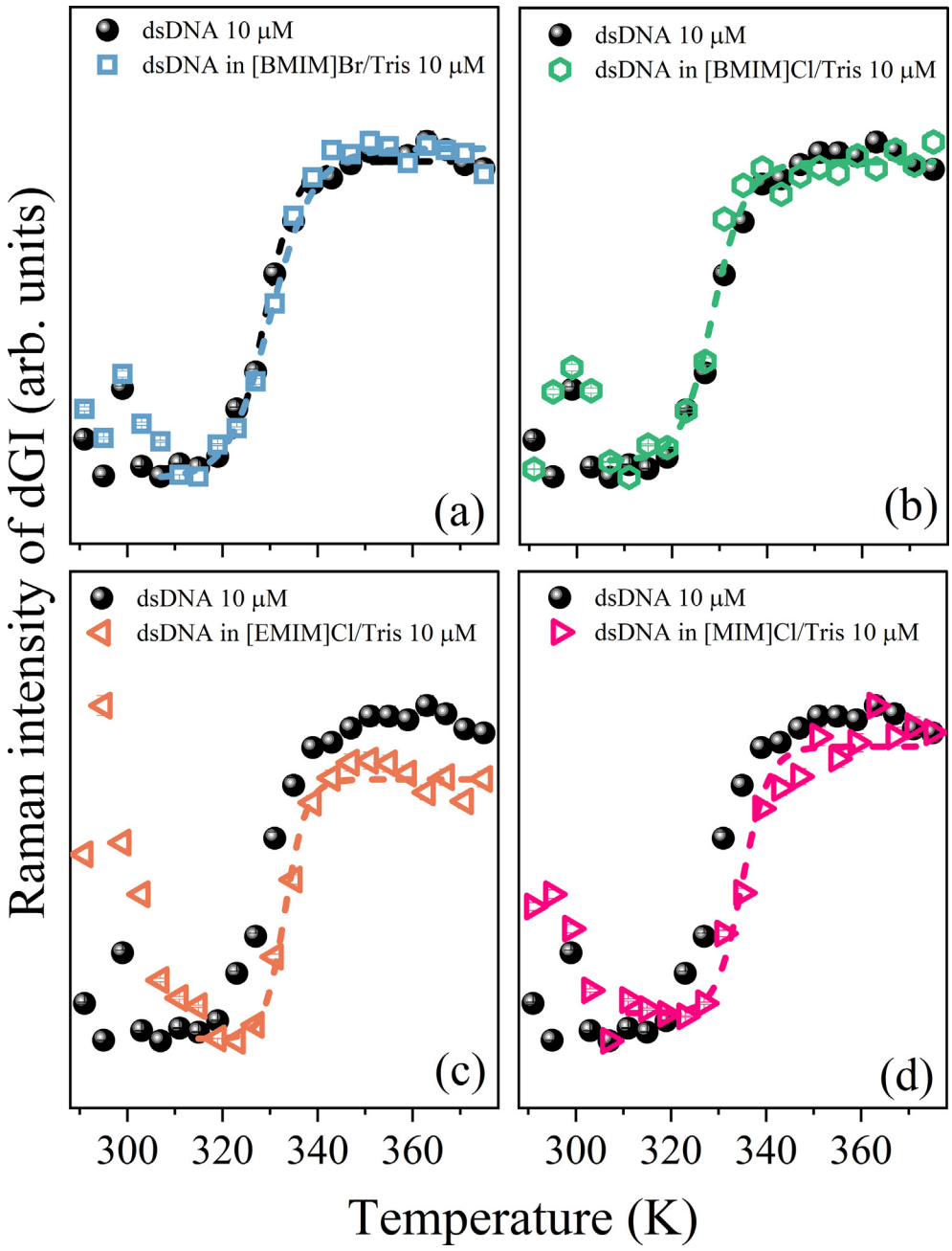

Fig. 2. Melting profile for Raman band dGI of dsDNA in Tris buffer in absence and presence of ionic liquids: (a) [BMIM]Br, (b) [BMIM]Cl, (c) [EMIM]Cl and (d) [MIM]Cl. All plots have been normalized to the minimum and the maximum values for a better comparison. Dashed lines are fitting of the experimental data by using Eq. (1), see details in the text.

(see Table 1). This supports the interpretation of the guanine transition temperature detected by UVRR as a process involving cooperative conformational changes specifically localized on dG base tracts of DNA, differently from the average melting process probed by UV absorption of DNA.

The $T_{G_{coop}}$ increment observed in the presence of cations with shorter alkyl-chain length on the imidazolium ring, i.e. [EMIM]Cl and [MIM]Cl, can be explained on the basis of recent experimental and simulation results indicating increasing charge delocalization in the imidazolium cation with the increasing length of the alkyl chain [75–77]. We can argue that such charge delocalization on the imidazolium ring may cause the weakening of electrostatic interaction between dsDNA backbones and -[BMIM]$^+$ compared

Table 1
Cooperative transition temperature $T_{G_{coop}}$ associated to partial disruption of guanine stacking estimated for dsDNA in Tris buffer in absence and presence of ILs. The $T_{G_{coop}}$ values have been obtained by fitting the experimental UVRR data of Fig. 2 with Eq. (1). The melting temperatures T_m calculated by UV absorbance experiments (data shown in Fig. S3) are reported for dsDNA in Tris and in [BMIM]Cl/Tris and [EMIM]Cl/Tris in the right column of the Table.

	$T_{G_{coop}}$ (K)	T_m (K)
dsDNA in Tris	329 ± 1	326.7 ± 0.5
dsDNA in [BMIM]Br/Tris	330 ± 1	
dsDNA in [BMIM]Cl/Tris	329 ± 1	327.0 ± 0.5
dsDNA in [EMIM]Cl/Tris	333 ± 1	328.3 ± 0.5
dsDNA in [MIM]Cl/Tris	335 ± 1	

to -[EMIM]$^+$ or -[MIM]$^+$ leading to different stabilization effects on the structure of DNA. The increment of $T_{G_{coop}}$ found for short alkyl chain imidazolium cations confirms the previous outcomes on large DNA molecules hydrated in imidazolium-based ILs [39] and is opposite to the results reported by Liu et al. [32] that suggest stronger intercalating interactions with DNA while increasing the length of the alkyl side chain in imidazolium cations. Our findings seem to support the conclusion of a predominant groove binding mechanism between IL cations and DNA [21,25,27,28,31,33] instead of semi-intercalation [32].

Besides the cooperative transition discussed above, the temperature profile for Raman band dGI of dsDNA shows a temperature-dependent increase of the intensity at about 299 K (Fig. 2) that clearly departs from the idealized two-state transition behavior detected by $T_{G_{coop}}$. This trend has been linked to the typical signature of non-cooperative structural changes occurring prior to the melting of DNA, i.e. pre-melting transformations already observed in oligonucleotides and large DNA molecules [37,64,67,69,70,72]. The substantial independence from the temperature of the UV absorbance of dsDNA in the pre-melting region (Fig. S3) confirms the localized nature of the dG residues conformational changes detected by UVRR. The pre-melting observed for dsDNA at about 299 K is probably correlated to structural changes such as enhanced base mobility and reversible rupture or weakening of inter-base H-bonds that perturb but do not destroy the guanine stacking interactions [64,78]. We can argue that the pre-melting transition detected by UVRR is associated with a conformational adjustment of the phosphate backbone of dsDNA induced by a partial disruption in the layer of hydration shell around double helix that affects both the backbone helical geometry and the inter-base interactions [72]. Interestingly, the plots in Fig. 2 point out that [EMIM]Cl and [MIM]Cl notably reduce the pre-melting temperature of dsDNA. This can be clarified by looking at the first-order derivatives of the dGI intensity temperature profiles for dsDNA in the absence and presence of ILs reported in Fig. S5. The maxima found in the temperature derivatives of Fig. S5 resemble the inflection points of the two-step trend of the dGI band observed for T$\gtrsim$310 K (i.e. $T_{G_{coop}}$ values reported in Table 1), while the points at which the derivatives change sign mark the pre-melting temperature characteristic of each analyzed system. We can note that for dsDNA dissolved in [EMIM]Cl/Tris and [MIM]Cl/Tris solution, the pre-melting temperature of the dG bases reduces from 299 to 295 and 293 K, respectively. This finding further supports the hypothesis of a stronger interaction between the imidazolium cations with shorter alkyl-chain length -[EMIM]$^+$ and -[MIM]$^+$ and the guanine residues in the structure of dsDNA, as confirmed by MD simulations results (see in the following).

Fig. 3 displays the temperature-dependence of the wavenumber position for the Raman bands at $\sim$ 1483, 1582 and 1332 cm^{-1} for dsDNA in Tris buffer in presence and absence of ILs.

The red-shift of the dGI mode (Fig. 3(a)) with increasing T reflects the formation of stronger H-bonds on the N7 site of dG [37,38,66]. This effect can be ascribed to the progressive substitution of base–base H-bonds with base-water H-bonds, promoted by the increment of thermal motion that might lower the frequency of the dGI mode. Remarkably, [MIM]Cl induces a significant further red-shift of the dGI band compared to the buffer solution, over all the explored T range (Fig. 3(a)). This finding is consistent with the "dehydration" effect operated by the ionic liquid [MIM]Cl on the structure of the duplex [25,27], whose cation experiences stronger interactions with the H-bonding sites of guanine than with water. Other Raman bands with predominant imidazole ring character are diagnostic of nucleotide conformations in DNA, such as the prominent signal at 1332 cm^{-1} observed in the spectrum of dsDNA [66,60]. This band downshifts with the increasing temperature for dsDNA, as shown in Fig. 3(b). We observe a stronger perturbation exerted by [EMIM]Cl than other ILs on the thermal pathway of the signal at 1332 cm^{-1}, which appears overall blue-shifted. This latter effect can be ascribed to the sensitivity of the Raman band at $\sim$ 1332 cm^{-1} to the local changes involving both dG and dA residues [60,62]. Similarly, the upshift revealed for the frequency position of the Raman band dGII of dsDNA as a function of temperature (Fig. 3(c)) is closely related to the partial disruption of guanine stacking occurring during the cooperative transition detected for dsDNA at about 330 K [37]. The strengthening of the double bonds of the guanine ring reflects the transition from the double- to the single-stranded structure of DNA during the melting, occurring both in the absence and presence of ILs (see Fig. 3(c)).

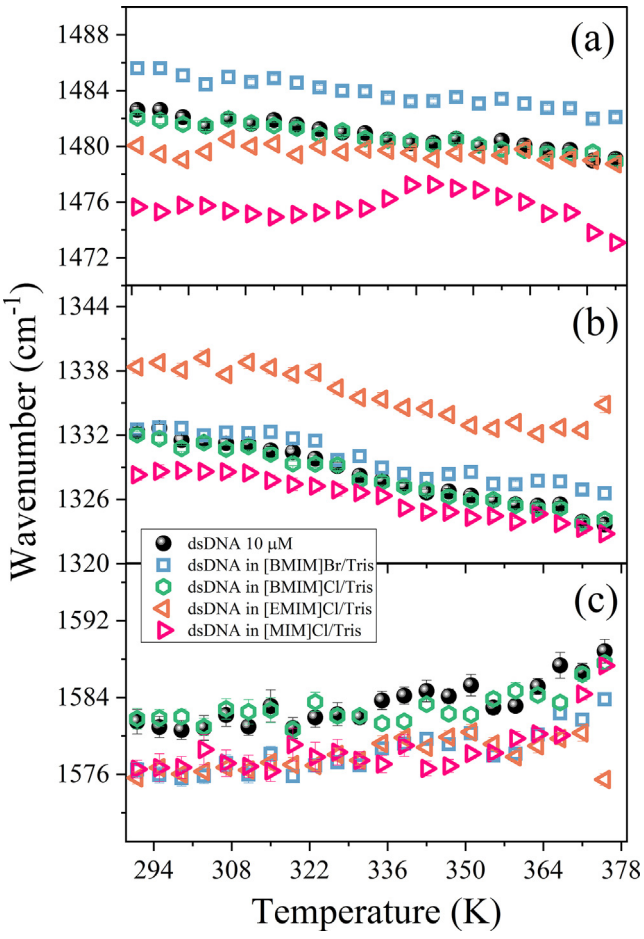

Fig. 3. Temperature evolution of central wavenumber position of the Raman bands at $\sim$ 1483 cm^{-1} (dGI) (a), $\sim$ 1332 cm^{-1} (dA,dG) (b) and 1582 cm^{-1} (dGII) (c) for dsDNA in Tris buffer in absence and presence of ILs. The plots have been derived from UVRR spectra collected using 250 nm as excitation wavelength.

3.2. Intermediate conformational states of dA-dT residues in hydrated ILs

The analysis of the UVRR spectra collected using 266 nm as excitation wavelength provides specific information on the thermally induced conformational changes of adenine dA and thymine dT residues in dsDNA. Indeed, with 266-nm as excitation wavelength, the ring vibrational bands assigned to the adenine dA residue mostly contribute to the spectrum of DNA [37,60]. The C = O stretching band of thymine dT, which is usually strongly overlapped with the same band of cytosine dC, exhibits an intensity

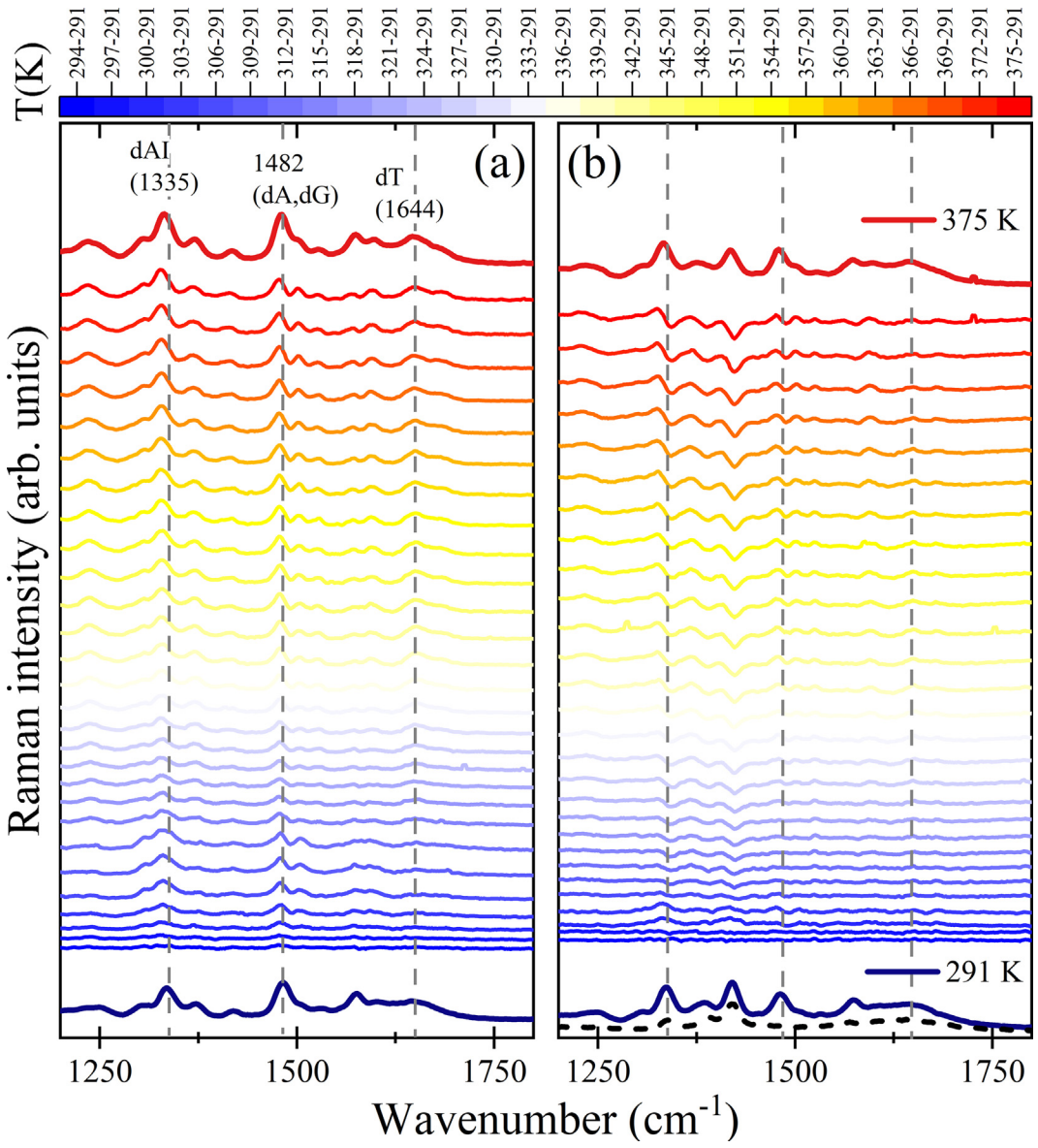

Fig. 4. 266 nm-excited Raman spectra of dsDNA (10 μM) in Tris buffer (a) and dsDNA in [EMIM]Cl/Tris (b) collected at 291 K (bottom trace) and 375 K (top trace); intermediate traces are the difference spectra computed by subtracting the spectrum measured at the lowest temperature from the spectrum at the indicated temperatures. The spectrum of [EMIM]Cl/Tris solution is also reported for comparison (dashed line in panel b).

of about three times greater than dC at 266 nm. Fig. 4 displays the temperature evolution of 266 nm-excited UVRR spectra for dsDNA in Tris buffer in absence and presence of [EMIM]Cl, as an example.

The Raman difference spectra reported in Fig. 4 evidence remarkable temperature induced changes in intensity and frequency for dsDNA Raman bands at ~ 1335, 1482 and 1644 cm^{-1}. The signal at ⌣ 1335 cm^{-1} (dAI) is attributed to the coupled stretching vibrations of N7 = C8 and C5- N7 bonds of adenine dA [60,79,80]. This mode is sensitive to dA nucleobase conformation [69] and to modifications of H-bonds at the N7 acceptor site of adenine [67,81]. At the excitation wavelength of 266 nm, the signal at ⌣ 1482 cm^{-1} contains comparable contributions arising from dA and dG residues [37]. The signal labeled as dT ~ 1644 cm^{-1} is attributed to coupled stretching of C4 = O and C5 = C6 bonds of the thymine dT residue and reflects any perturbations occurring at the C = O site of dT base [70,82,83] (see Fig. S2(b) for the numbering of atoms). The comparison between UVRR spectra of dsDNA in the absence and presence of ILs (Fig. 4(a)-(b)) suggests that the DNA duplex follows a different thermal pathway when in hydrated ILs. This can be well rationalized by looking at the temperature dependence of the dAI band intensity. Fig. 5 shows the evolution of the Raman hyperchromism for the signal dAI ⌣ 1335 cm^{-1} that, similarly to the dGI band intensity, reflects the partial unstacking of dA bases during the melting of DNA.

As a first remark, the intensity of the dAI band of dsDNA exhibits a temperature dependence that slightly departs from the ideal two-state behavior representative of the cooperative transition detected for the dGI band in the same temperature range (see Fig. 2). The trend reported in Fig. 5 for the dAI band suggests that even rather minor temperature variations may give rise to local conformational changes in the structure of dsDNA that primarily involve adenine bases [37,64,70,72]. More quantitative information on the structural modifications and on the thermodynamic parameters experienced by dA residues in the absence and presence of ILs can be traced back by the first-order derivative of the temperature profiles of dAI intensity (Fig. S6). The derivative curves evidence, for all systems analyzed, a reversible pre-melting transformation for temperature below 315 K and a more

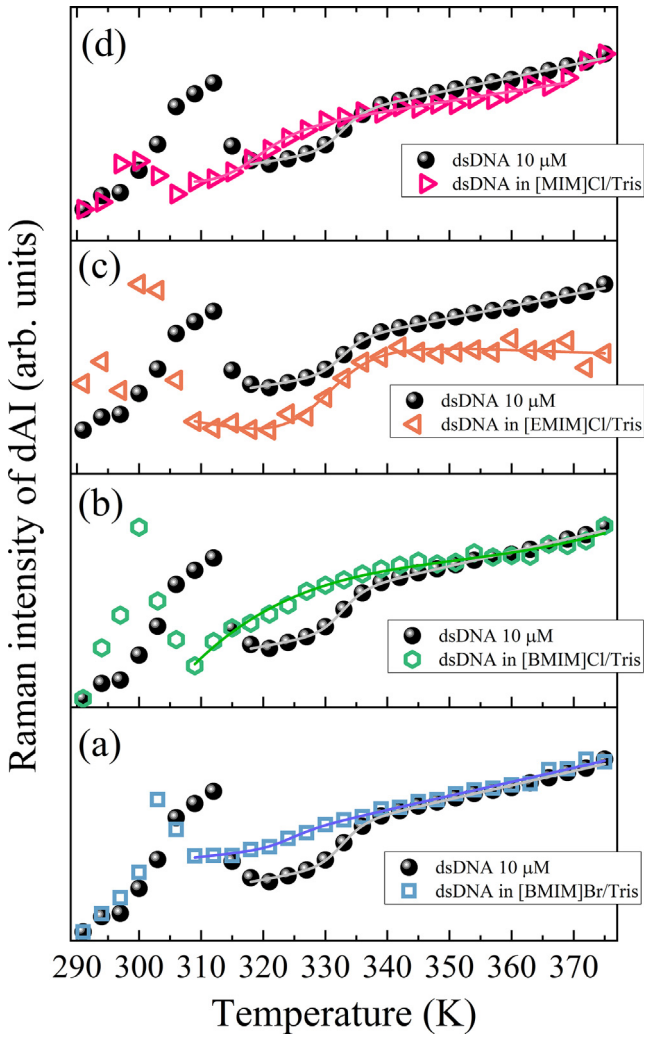

Fig. 5. Melting profile for Raman band dAI of dsDNA in Tris buffer in absence and presence of ionic liquids: (a) [BMIM]Br, (b) [BMIM]Cl, (c) [EMIM]Cl and (d) [MIM]Cl. All the plots have been normalized to the minimum and the maximum values for a better comparison. Full lines are fitting of the experimental data by using Eq. (2), see details in the text.

cooperative transition occurring at a higher temperature ($T_{A_{coop}}$). The monotonic temperature dependence of the dAI band above 315 K suggests the occurrence of a simple two-stage structural process involving adenine-pairs along the dsDNA thermal pathway, differently from the multiple intermediate stacking arrangements detected for dA in large molecules of DNA [39]. This cooperative transition probably involves a partial disruption of the adenine stacking interactions that precedes the separation of DNA strands during the melting. The values of $T_{A_{coop}}$ for dsDNA in Tris buffer in the absence and presence of ILs can be estimated by the fitting of the experimental trends reported in Fig. 5 with a similar two-state law [37,38]:

$$I_{dAI}(T) = \frac{C + m_C \cdot T + (D + m_D \cdot T) \cdot e^{\frac{\Delta H_A}{R}\left(\frac{1}{T_{A_{coop}}} - \frac{1}{T}\right)}}{1 + e^{\frac{\Delta H_A}{R}\left(\frac{1}{T_{A_{coop}}} - \frac{1}{T}\right)}} \quad (2)$$

where C and D represent the lower and upper limit of the ordinate (Raman spectral dA band intensity), R is the gas constant, ΔH_A and $T_{A_{coop}}$ are the enthalpy variation and the temperature associated with the cooperative transition of adenine-pairs. The parameters m_c and m_D have been introduced in Eq. (2) to account for the linear temperature dependence of the band intensity in the pre- and post-melting regions, respectively. The values of $T_{A_{coop}}$ for dsDNA in Tris and in ILs/Tris solutions are reported in Table 2 and point out a general decrement of the dA cooperative transition temperature exerted by all the ILs considered in this study.

Fig. 6 summarizes the values estimated for the pre-melting and the cooperative transitions temperatures associated to guanine (T_G) and adenine (T_A) residues of dsDNA in absence and presence of ILs.

We observe a notable difference in the thermally induced behavior of guanine and adenine residues in dsDNA involved in cooperative structural transformations occurring at a slightly higher temperature for dG compared to dA. More interestingly, the effect on the transition temperature is the opposite for the two residues, i.e. an increment of T_G, observed especially for ILs with a shorter alkyl-chain length of imidazolium cations, and a general decrement of T_A common to all the ILs.

The experimental results indicate that both dG and dA bases in the structure of dsDNA are involved in pre-melting conformational transformations occurring at specific temperatures below 315 K. Consistently with similar pre-melting phenomena observed in poly(dA–dT) · poly(dA–dT) double-helical B DNA [69,70,83], the reversible increment of the dAI intensity at 310 K may be related to the stabilization of extra amount of propeller twist between the A-T base planes through the formation of a third hydrogen bond cross-strand between consecutive dA - dT pairs [70]. Interestingly, Fig. 6 points out that all considered ILs induce a pronounced reduction of the characteristic temperature associated with the pre-melting transformation of dA bases in dsDNA, with a more marked effect for ILs with chloride as the anion. This finding can be rationalized by considering the predicted binding capability of ions with the minor groove of DNA that determines DNA deformations, such as bending of dA-dT pairs [84,85]. The effect driven by the imidazolium-based ILs with Cl^- as anion suggests a selective strong interaction of this anion with the adenine bases on the structure of dsDNA. The analysis of the temperature behavior of the 1482 cm^{-1} band intensity (dA, dG) reported in the Supplementary Information section (Fig. S7) confirms the stronger influence operated by ILs with Cl^- as the anion in comparison with Br^- on the pre-melting of dA residues.

In the wavenumber region 1300–1500 cm^{-1}, the Raman bands of dsDNA shift to lower frequency upon the increment of the temperature, both in the absence and presence of ILs. This is clearly visible in Fig. 7(a) and (b) for the signals at ~ 1335 cm^{-1} (dAI) and at ~ 1482 cm^{-1} (dA, dG), mainly described by vibrations arising from purine residues.

The frequency of the oscillators associated with these Raman signals is sensitive to the different hydrogen bonding states on the proton-acceptor N7 site, mostly of adenine residues [62,66,69,80,81]. The progressive weakening of H-bonds at the acceptor sites N7 of adenine with increasing temperature may explain the concerted red-shifts observed for the Raman signals in Fig. 7(a) and (b) [69,81]. This is due to the replacement of

Table 2
Cooperative transition temperature $T_{A_{coop}}$ associated to partial disruption of adenine stacking interactions estimated for dsDNA in Tris buffer in absence and presence of ILs. The $T_{A_{coop}}$ values have been obtained by fitting of the experimental data of Fig. 5 with Eq. (2).

	$T_{A_{coop}}$ (K)
dsDNA in Tris	333 ± 1
dsDNA in [BMIM]Br/Tris	324 ± 1
dsDNA in [BMIM]Cl/Tris	324 ± 1
dsDNA in [EMIM]Cl/Tris	330 ± 1
dsDNA in [MIM]Cl/Tris	318 ± 1

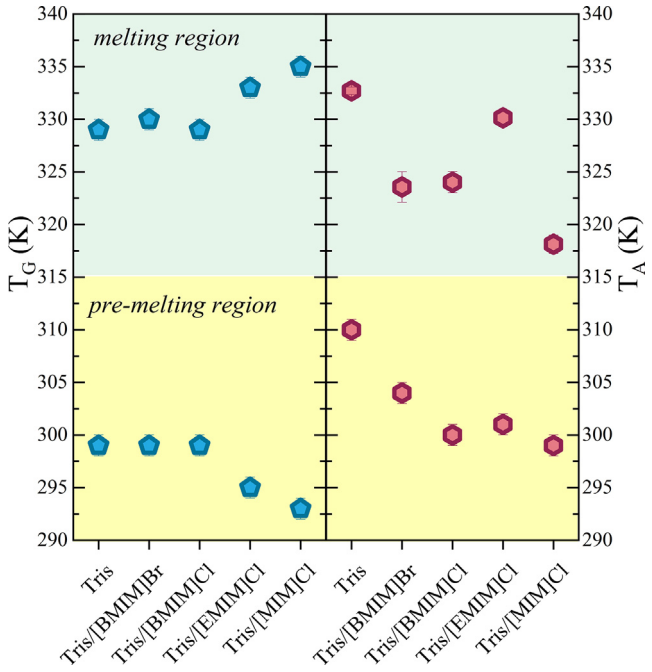

Fig. 6. The pre-melting and cooperative transitions temperatures localized on guanine (T_G, cyan symbols) and adenine (T_A, magenta symbols) nucleobases of dsDNA as a function of the different type of solvents, i.e. Tris buffer or ILs/Tris solutions.

inter-adenine hydrogen bonds with weaker adenine-water hydrogen bonds, promoted by the progressive exposition to the solvent of the DNA strands dA residues during the melting. Fig. 7(a) and (b) point out no significant modifications in the frequency of the Raman bands attributed to dA induced by ILs. This issue could be consistent with the assumption that the binding between ILs anions and the minor groove of DNA chiefly induces base tilting rather than the rupture of hydrogen bonds on adenine residues in dA-dT pairs. Fig. 7(c) displays the temperature dependence of the wavenumber position for the dT band whose strength of oscillation accounts for any perturbations occurring at the C4 = O site of thymine residue [60,70,81]. The marked upshift of this mode observed before the melting at ~ 335 K can be correlated with a decrease in H-bonding strength on the C = O site of thymine during the cooperative transition detected at this temperature for dA residues [37,70]. The relatively large blue-shift (about 7 cm^{-1}) observed for the dT band as a function of temperature is consistent with the existence in the duplex structure of dsDNA of a cross-strand three-centered H-bonds between dA and dT bases [70]. Since the pre-melting transition is primarily attributed to changes of propeller twisting and to the strength of the cross-strand three-centered H-bonds, the data reported in Fig. 7(c) seem to suggest a negligible perturbation operated by ILs on the extent of these three-centered H-bonding.

3.3. Structure of dsDNA in hydrated ILs

By MD simulations, we analyzed the structure of the dsDNA along the simulation trajectories (100 ns) to check if the DNA could maintain its native B-conformation in the hydrated ILs considered in this study ([MIM]Cl, [EMIM]Cl, [BMIM]Cl and [BMIM]Br). The structural stability of the dsDNA was investigated by comparing the root mean square deviation (RMSD) values of DNA solvated in pure water and in the hydrated ILs solutions relative to the initial position in the crystal B-form structure (Fig. 8).

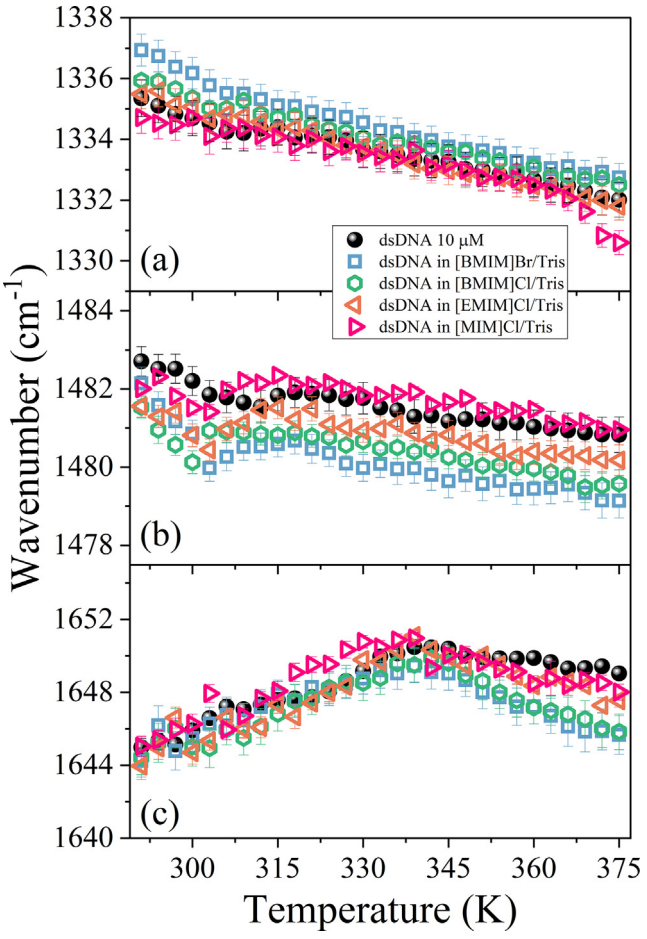

Fig. 7. Temperature evolution of central wavenumber position of the Raman bands at ~ 1335 cm^{-1} (dAl) (a), ~ 1482 cm^{-1}(dA,dG) (b) and ~ 1644 cm^{-1}(dT) (c) for dsDNA in Tris buffer in absence and presence of ILs. The plots have been derived from UVRR spectra collected using 266 nm as excitation wavelength.

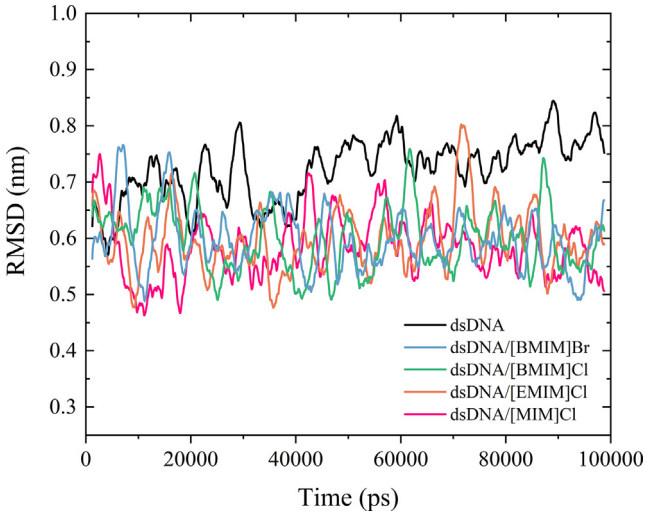

Fig. 8. Root-mean-square deviation (RMSD, nm) of dsDNA solvated in the four hydrated ILs (54 mM) and in pure water.

Over the 100 ns, the average RMSD values in hydrated [MIM]Cl, [EMIM]Cl, [BMIM]Cl, [BMIM]Br and pure water are 0.582 nm, 0.596 nm, 0.598 nm, 0.598 nm and 0.721 nm, respectively. We found all the average RMSD values calculated for DNA in each

hydrated IL to be lower than the value observed in the pure water solution. Reducing the alkyl-chain length on the imidazolium cation from 1-butyl-3-methylimidazolium to 1-methylimidazolium seems to slightly decrease the average RMSD value of the DNA. This indicates that the alkyl chain lengths of the cations have a small influence on the stability of the DNA at room temperature, consistently with the experimental evidence.

Fig. 9 shows the distribution of 1-methylimidazolium cations on the surface of dsDNA. This picture illustrates that populations of cations are located near DNA phosphate groups due to the charge attraction and are also associated with the major and minor grooves of DNA. According to this figure, we assume the cations disrupted the hydration shells, entered the minor and major grooves and remained bound to the grooves without disturbing the helical structure of dsDNA. We may infer that the hydrogen bond between the cation and grooves helps stabilize the DNA.

3.4. Role of hydration shells

The stability of DNA mainly depends on the water content or on the properties of hydration shells around DNA. In fact, the hydration shells play a vital role in stabilizing or destabilizing DNA and its conformational dynamics [27]. Fig. 10 displays the distribution of 1-methylimidazolium cations and water molecules in the solvation layers of dsDNA, defined as a shell of 0.35 nm.

According to this figure, 1-methylimidazolium cations penetrate the hydration layer of the DNA and take part in the solvation mechanism. As shown in Fig. 10, the cations interact with the various regions of DNA, thereby the cations are trapped in the DNA. Consequently, water molecules are not able to diffuse inside the helical structure easily [25] and, the disturbing of DNA conformation by water diffusion is reduced. Such partial dehydration of the DNA by cations could also prevent hydrolytic reactions such as depurination and deamination, as previously suggested by other authors [25,27]. Moreover, the number of water molecules in DNA solvation shell as a function of the simulation time have been calculated to gain more information about the scale of water displacement by the alkyl imidazolium cations. Fig. 11 shows the number of water molecules around the major groove in the aqueous solution of [MIM]Cl, [EMIM]Cl, [BMIM]Cl and [BMIM]Br.

According to this plot, the number of water molecules which are present within 3.5 Å around the major groove of DNA is lowest in hydrated [MIM]Cl solution. In other words, more water molecules were stripped off by 1-methylimidazolium cations from

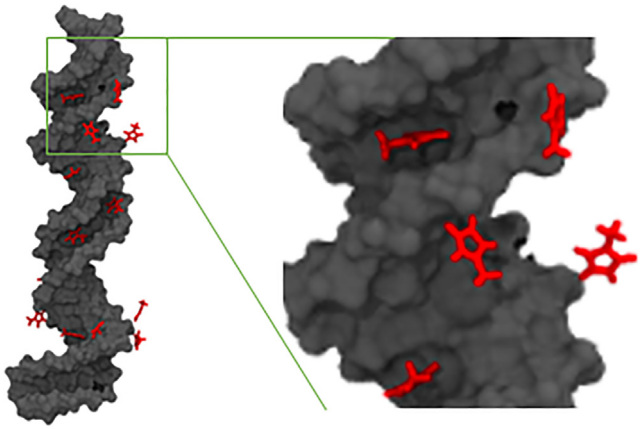

Fig. 9. Representative distribution of 1-methylimidazolium cations that shows their association with the DNA phosphate groups, major and minor grooves in the aqueous solution of [MIM]Cl (54 mM). Color coding: gray, DNA; red, 1-methylimidazolium cations.

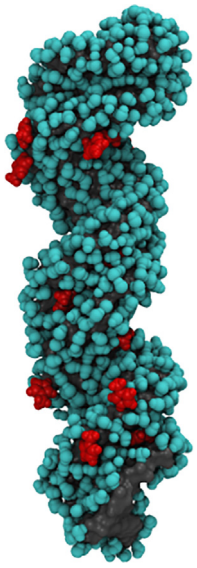

Fig. 10. Representative distribution of the populations of 1-methylimidazolium cations and water molecules within 0.35 nm of DNA surface in the aqueous solution of [MIM]Cl (54 mM). Color coding: gray, DNA; cyan, water and red, 1-methylimidazolium cation.

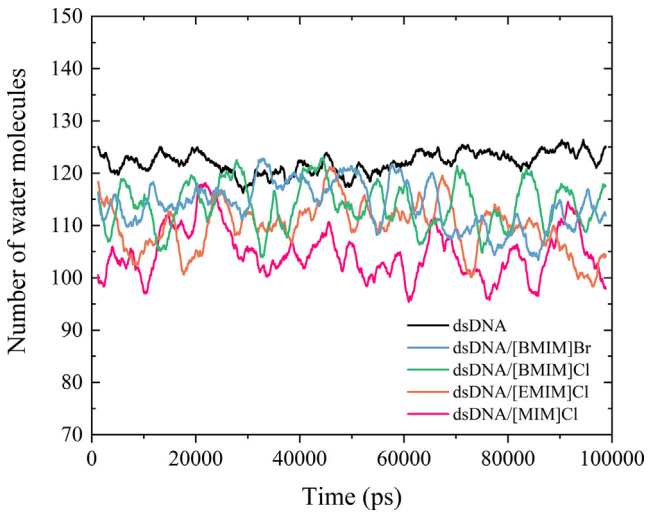

Fig. 11. The number of water molecules which are present within 3.5 Å around the dsDNA major groove in the presence of different hydrated ILs (concentration of 54 mM of IL in water) throughout the simulation trajectory.

DNA surface. This finding further supports the experimental UVRR data that suggest a stronger interaction of guanine residues in the structure of dsDNA with imidazolium cations with shorter alkyl-chain length.

3.5. Binding characteristics of ILs–dsDNA

In this study, various radial distribution function (RDFs) of ILs around DNA (major groove) were explored and compared to find the binding pattern of ILs to DNA. Fig. 12 shows the RDF of center of mass (COM) of the imidazolium ring around the major groove of DNA in different hydrated imidazolium ILs solutions. According to this figure, the distribution of cations in the major groove is the highest in the aqueous solution of [MIM]Cl, meaning the penetration of [MIM] cations into the DNA major groove. As previously mentioned, the interaction of the cationic head groups with the

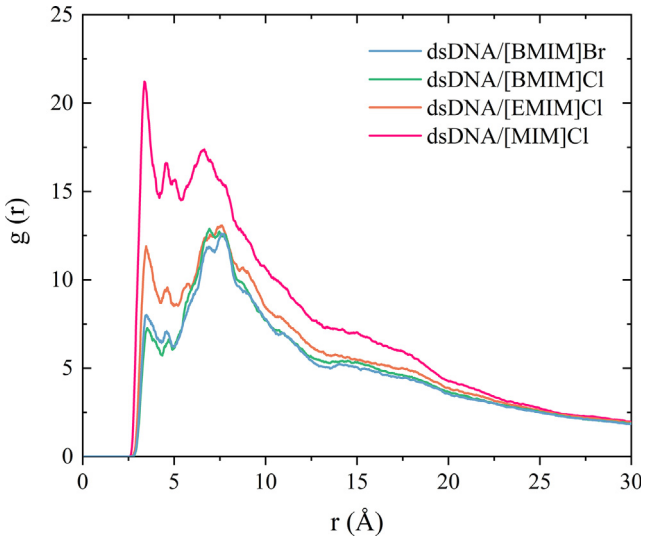

Fig. 12. The RDF of COM of the imidazolium ring around major groove of the DNA in different hydrated imidazolium ILs solutions (54 mM). The N7 site for the major groove was considered for calculating the RDFs.

DNA (the major groove) increases with decreasing alkyl chain length of the ILs. Then, we may assume that the interaction of shorter alkyl-chain length on the imidazolium ring ($[MIM]^+$) with the major groove and the partial dehydration of DNA are the key factors that stabilize DNA in hydrated ILs, consistently with the experimental UVRR results.

Moreover, Fig. 12 shows that, switching from chloride to bromide ion in [BMIM] ionic liquids, the interaction of [BMIM] cation with major groove of dsDNA is slightly more pronounced. It is worthy to mention that, as DNA is a polyanion polymer, the anions are not well-distributed on the surface of DNA. The distribution of anions around the DNA was not reported in this study. However, the DNA was simulated in two hydrated [BMIM]-based ILs ([BMIM]Cl and [BMIM]Br) to investigate the effects of the anion on the DNA stability. According to Fig. 11, the average number of water molecules present within 3.5 Å around the major groove of DNA in [BMIM]Br and [BMIM]Cl water solutions are approximately the same and no meaningful difference was observed. This issue can be explained considering that the concentration of water in the solution is more than 50 mol/L and the changes of its concentration around dsDNA due to different ions is negligible. The concentration of ions such as counter-ions is low according to counter-ion condensation theory introduced by Manning which discusses the importance of charge distribution of polynucleotides in electrolyte solutions [86] where a fraction of counter-ions is associated with the DNA. In this viewpoint, also Young and coworkers [87] from MD simulations, showed that a Na^+ ion was in the minor groove more than half of the trajectory. In addition, MD simulations of Ponomarev et al. [88] in dilute aqueous solutions with Na^+ counter-ions showed that the effect of ion convergence on the conformational and helicoidal parameters of DNA and the effect of ions on the width of the minor groove of the DNA are important. According to what was mentioned above, counter-ions have a significant effect on DNA structure axis curvature and ligand interaction [88]. Due to the fact that neutralization [88] of DNA in solutions can affect the structure of DNA during the MD simulations, therefore, DNA molecule was balanced by the addition of 58Na^+ counter-ions to the systems for neutralization while the addition of positively charged imidazolium ions could compensate the negative charge DNA.

4. Summary and conclusions

The ability of ionic liquids in stabilizing and preserving the conformation of nucleic acids is important in the field of biology, medical diagnostics and biotechnology, especially for DNA storage and handling. Several studies predicted that aqueous solutions of ILs with cations based on imidazolium enable to improve the structural stability of DNA but the dominant interactions between this class of ILs and nucleic acids have still to be fully understood. In this regard, many experimental techniques of analysis of DNA suffer from the missing of sequence specificity and are less sensitive to transitions which do not involve changes of the number of closed base pairs. SR-UVRR technique is able to differentiate contributions of single nucleobases interactions to the structural transformation of DNA duplexes during thermal pathway. In this work, we have implemented SR-UVRR experiments and molecular dynamics simulations for testing the nature of the conformational transitions along the melting pathway of a synthetic 30-base pair duplex affected by the presence of imidazolium-based ILs. Our experimental and simulation findings consistently suggest the predominance of a groove binding mechanism between the imidazolium cations and dsDNA, with a preferential interaction established between guanine residues and the imidazolium cations with shorter alkyl-chain length. This seems to be a common behavior observed for both short and large DNA molecules hydrated in imidazolium-based ILs. UVRR data evidence that even rather small temperature variations may give rise to reversible premelting structural transitions that involve both dG and dA residues in the structure of dsDNA. These conformational changes, not detected by UV absorption melting curves, are associated with reversible rupture or weakening of H-bonds in the double-stranded structure as well as bases tilting that are activated at lower temperature for guanine residues compared to adenine ones. The binding of Cl^- anions with the minor groove of DNA especially induces the base tilting rather than the rupture of hydrogen bonds on adenine residues in dA-dT pairs. According to the MD simulation results, electrostatic interactions drive the stronger attraction between the cations in the aqueous solution of [MIM]Cl and the DNA major groove. We can speculate that such partial dehydration of the DNA by cations prevents hydrolytic reactions and increases the conformational stability of the DNA in comparison with other hydrated ILs.

CRediT authorship contribution statement

Fatemeh Fadaei: Investigation, Data curation. **Mariagrazia Tortora:** Investigation, Data curation. **Alessandro Gessini:** Methodology, Software. **Claudio Masciovecchio:** Funding acquisition, Supervision. **Sara Catalini:** Investigation, Data curation. **Jacopo Vigna:** Investigation, Data curation. **Ines Mancini:** Investigation, Writing – review & editing. **Andrea Mele:** Writing – review & editing. **Jan Vacek:** Investigation, Writing – review & editing. **David Reha:** Data curation. **Babak Minofar:** Investigation, Supervision, Writing – review & editing. **Barbara Rossi:** Conceptualization, Supervision, Writing – original draft.

Declaration of Competing Interest

The authors declare that they have no known competing financial interests or personal relationships that could have appeared to influence the work reported in this paper.

Acknowledgments

MT thanks the European Regional Development Fund and Interreg V-A Italy Austria 2014–2020 through the Interreg Italy-Austria project ITAT 1059 InCIMa4 "InCIMa for Science and SMEs". We acknowledge Elettra Sincrotrone Trieste for providing access to its synchrotron radiation facilities and for financial support (proposal number 20195426). The authors acknowledge the CERIC-ERIC Consortium for the access to experimental facilities and financial support (proposal 20202148). FF and BM thank computational resources which were supplied by the project "e-Infrastruktura CZ" (e-INFRA LM2018140) provided within the program Projects of Large Research, Development and Innovations Infrastructures.

Appendix A. Supplementary data

Supplementary data to this article can be found online at https://doi.org/10.1016/j.molliq.2021.118350.

References

[1] E. Lattuada, M. Leo, D. Caprara, L. Salvatori, A. Stoppacciaro, F. Sciortino, P. Filetici, DNA-GEL, novel nanomaterial for biomedical applications and delivery of bioactive molecules, Front. Pharmacol. 11 (2020) 01345, https://doi.org/10.3389/fphar.2020.01345.
[2] H. Joshi, A. Kaushik, N.C. Seeman, P.K. Maiti, Nanoscale structure and elasticity of pillared DNA nanotubes, ACS Nano 10 (8) (2016) 7780–7791, https://doi.org/10.1021/acsnano.6b03360.
[3] Y. Murakami, M. Maeda, DNA-responsive hydrogels that can shrink or swell, Biomacromolecules 6 (6) (2005) 2927–2929, https://doi.org/10.1021/bm0504330.
[4] S.D. Patil, D.G. Rhodes, D.J. Burgess, DNA-based therapeutics and DNA delivery systems: a comprehensive review, AAPS J. 7 (1) (2005) E61–E77, https://doi.org/10.1208/aapsj070109.
[5] M.J. Heller, DNA microarray technology: devices, systems, and applications, Annu. Rev. Biomed. Eng. 4 (1) (2002) 129–153, https://doi.org/10.1146/annurev.bioeng.4.020702.153438.
[6] O. Fedrigo, G. Naylor, A gene-specific DNA sequencing chip for exploring molecular evolutionary change, Nucleic Acids Res. 32 (2004) 1208–1213, https://doi.org/10.1093/nar/gkh210.
[7] C. Morishima, M. Chung, K.W. Ng, D.J. Brambilla, D.R. Gretch, Strengths and limitations of commercial tests for hepatitis C virus RNA quantification, J. Clin. Microbiol. 42 (1) (2004) 421–425, https://doi.org/10.1128/JCM.42.1.421-425.2004.
[8] J. Zheng, J.J. Birktoft, Y.i. Chen, T. Wang, R. Sha, P.E. Constantinou, S.L. Ginell, C. Mao, N.C. Seeman, From molecular to macroscopic via the rational design of a selfassembled 3D DNA crystal, Nature 461 (7260) (2009) 74–77, https://doi.org/10.1038/nature08274.
[9] R.J. Macfarlane, B. Lee, M.R. Jones, N. Harris, G.C. Schatz, C.A. Mirkin, Nanoparticle superlattice engineering with DNA, Science 334 (6053) (2011) 204–208.
[10] T. Lindahl, B. Nyberg, Rate of depurination of native deoxyribonucleic acid, Biochemistry 11 (19) (1972) 3610–3618, https://doi.org/10.1021/bi00769a018.
[11] W.K. Pogozelski, T.D. Tullius, Oxidative strand scission of nucleic acids: Routes initiated by hydrogen abstraction from the sugar moiety, Chem. Rev. 98 (1998) 1089–1108, https://doi.org/10.1021/cr960437i.
[12] J. Cadet, T. Delatour, T. Douki, D. Gasparutto, J.-P. Pouget, J.-L. Ravanat, S. Sauvaigo, Hydroxyl radicals and DNA base damage, Mutat. Res./Fundam. Mol. Mech. Mutagen. 424 (1-2) (1999) 9–21, https://doi.org/10.1016/S0027-5107(99)00004-4.
[13] H. Tateishi-Karimata, N. Sugimoto, Structure, stability and behaviour of nucleic acids in ionic liquids, Nucleic Acids Res 42 (14) (2014) 8831–8844.
[14] Z. Lei, B. Chen, Y.-M. Koo, D.R. MacFarlane, Introduction: Ionic Liquids, Chem. Rev. 117 (10) (2017) 6633–6635.
[15] A. Benedetto, P. Ballone, Room temperature ionic liquids meet biomolecules: a microscopic view of structure and dynamics, ACS Sustain. Chem. Eng. 4 (2) (2016) 392–412, https://doi.org/10.1021/acssuschemeng.5b01385.
[16] K.S. Egorova, E.G. Gordeev, V.P. Ananikov, Biological activity of ionic liquids and their application in pharmaceutics and medicine, Chem. Rev. 117 (10) (2017) 7132–7189, https://doi.org/10.1021/acs.chemrev.6b00562.
[17] D. Saha, A. Mukherjee, Effect of water and ionic liquids on biomolecules, Biophys. Rev. 10 (3) (2018) 795–808, https://doi.org/10.1007/s12551-018-0399-2.
[18] M. Sivapragasam, M. Moniruzzaman, M. Goto, Recent advances in exploiting ionic liquids for biomolecules: Solubility, stability and applications, Biotechnol. J. 11 (2016) 1000–1013, https://doi.org/10.1002/biot.201500603.
[19] S.K. Shukla, J.-P. Mikkola, Use of ionic liquids in protein and DNA chemistry, Front. Chem. 8 (2020), https://doi.org/10.3389/fchem.2020.598662 598662.
[20] M.J. Earle, K.R. Seddon KR, Ionic liquids. Green solvents for the future, Pure Appl Chem 72 (2000) 1391–1398 doi: 10.1351/pac200072071391
[21] E.A. Oprzeska-Zingrebe, J. Smiatek, Aqueous ionic liquids in comparison with standard co-solutes Differences and common principles in their interaction with protein and DNA structures, Biophys. Rev. 10 (3) (2018) 809–824, https://doi.org/10.1007/s12551-018-0414-7.
[22] H. Tateishi-Karimata, N. Sugimoto, Biological and nanotechnological applications using interactions between ionic liquids and nucleic acids, Biophys. Rev. 10 (3) (2018) 931–940, https://doi.org/10.1007/s12551-018-0422-7.
[23] K.S. Egorova, A.V. Posvyatenko, S.S. Larin, V.P. Ananikov, Ionic liquids: prospects for nucleic acid handling and delivery, Nucleic Acids Res. 49 (3) (2021) 1201–1234, https://doi.org/10.1093/nar/gkaa1280.
[24] R. Vijayaraghavan, A. Izgorodin, V. Ganesh, M. Surianarayanan, D. MacFarlane, Long-term structural and chemical stability of DNA in hydrated ionic liquids, Angew. Chem., Int. Ed. 49 (9) (2010) 1631–1633, https://doi.org/10.1002/anie.200906610.
[25] A. Chandran, D. Ghoshdastidar, S. Senapati, Groove binding mechanism of ionic liquids: A key factor in long-term stability of DNA in hydrated ionic liquids, J. Am. Chem. Soc. 134 (50) (2012) 20330–20339, https://doi.org/10.1021/ja304519d.
[26] L. Cardoso, N.M. Micaelo, DNA molecular solvation in neat ionic liquids, Chem. Phys. Chem 12 (2) (2011) 275–277, https://doi.org/10.1002/cphc.201000645.
[27] K. Jumbri, M.B. Abdul Rahman, E. Abdulmalek, H. Ahmad, N.M. Micaelo, An insight into structure and stability of DNA in ionic liquids from molecular dynamics simulation and experimental studies, Phys. Chem. Chem. Phys. 16 (27) (2014) 14036–14046, https://doi.org/10.1039/C4CP01159G.
[28] K. Jumbri, M. B. Abdul Rahman, E. Abdulmalek, H. Ahmada, N. M. Micaelo, An insight into structure and stability of DNA in ionic liquids from molecular dynamics simulation and experimental studies, Phys. Chem. Chem. Phys. 16 (2014) 14036-14046
[29] A. Pabbathi, A. Samanta, Spectroscopic and molecular docking study of the interaction of DNA with a morpholinium ionic liquid, J. Phys. Chem. B 119 (34) (2015) 11099–11105, https://doi.org/10.1021/acs.jpcb.5b02939.
[30] H. Zhao, DNA stability in ionic liquids and deep eutectic solvents: DNA stability in ionic liquids and deep eutectic solvents, J. Chem. Technol. Biotechnol. 90 (1) (2015) 19–25.
[31] Y. Ding, L. Zhang, J.u. Xie, R. Guo, Binding Characteristics and Molecular Mechanism of Interaction between Ionic Liquid and DNA, J. Phys. Chem. B 114 (5) (2010) 2033–2043, https://doi.org/10.1021/jp9104757.
[32] H. Liu, Y. Dong, J. Wu, C. Chen, D. Liu, Q. Zhang, S. Du, Evaluation of interaction between imidazolium-based chloride ionic liquids and *calf thymus* DNA, Sci. Total Environ. 1–7 (2016) 566–567, https://doi.org/10.1016/j.scitotenv.2016.05.087.
[33] P.K. Singh, J. Sujana, A.K. Mora, S. Nath, Probing the DNA–ionic liquid interaction using an ultrafast molecular rotor, J. Photoch. Photobiol. A 246 (2012) 16–22, https://doi.org/10.1016/j.jphotochem.2012.07.006.
[34] Z. Meng, T. Kubar, Y. Mu, F. Shao, A Molecular Dynamics-Quantum Mechanics Theoretical Study of DNA-Mediated Charge Transport in Hydrated Ionic Liquids, J. Chem. Theory Comput. 14 (5) (2018) 2733–2742, https://doi.org/10.1021/acs.jctc.7b0120110.1021/acs.jctc.7b01201.s002.
[35] A.N. Bowers, M.J. Trujillo-Rodríguez, M.Q. Farooq, J.L. Anderson, Extraction of DNA with magnetic ionic liquids using in situ dispersive liquid–liquid microextraction, Anal. Bioanal. Chem. 411 (28) (2019) 7375–7385, https://doi.org/10.1007/s00216-019-02163-9.
[36] A. Garai, D. Ghoshdastidar, S. Senapati, P.K. Maiti, Ionic liquids make DNA rigid, J. Chem. Phys. 149 (4) (2018) 045104, https://doi.org/10.1063/1.5026640.
[37] C. Bottari, S. Catalini, P. Foggi, I. Mancini, A. Mele, D.R. Perinelli, A. Paciaroni, A. Gessini, C. Masciovecchio, B. Rossi, Base-specific pre-melting and melting transitions of DNA in presence of ionic liquids probed by synchrotron-based UV Resonance Raman scattering, J. Mol. Liq. 330 (2021) 115433, https://doi.org/10.1016/j.molliq.2021.115433.
[38] C. Bottari, I. Mancini, A. Mele, A. Gessini, C. Masciovecchio, B. Rossi, Conformational stability of DNA in hydrated ionic liquid by synchrotron-based UV resonance raman, Proc. SPIE 11086, UV and Higher Energy Photonics, From Materials to Applications 110860Q (2019), https://doi.org/10.1117/12.2529077.
[39] B. Rossi, M. Tortora, S. Catalini, J. Vigna, I. Mancini, A. Gessini, C. Masciovecchio, A. Mele, Phys. Chem. Chem. Phys. (2021), https://doi.org/10.1039/D1CP01970H.
[40] D. Saha, M. Kulkarni, A. Mukherjee, Water modulates the ultraslow dynamics of hydrated ionic liquids near CG rich DNA: consequences for DNA stability, Phys. Chem. Chem. Phys. 18 (47) (2016) 32107–32115, https://doi.org/10.1039/C6CP05959G.
[41] F. Bianchi, L. Comez, R. Biehl, F. D'Amico, A. Gessini, A.M. Longo, C. Masciovecchio, C. Petrillo, A. Radulescu, B. Rossi, F. Sacchetti, F. Sebastiani, N. Violini, A. Paciaroni, Structure of human telomere G-quadruplex in the presence of a model drug along the thermal unfolding pathway, Nucleic Acids Res. 46 (22) (2018) 11927–11938, https://doi.org/10.1093/nar/gky1092.
[42] L. Comez, F. Bianchi, V. Libera, M. Longo, C. Petrillo, F. Sacchetti, F. Sebastiani, F. D'Amico, B. Rossi, A. Gessini, C. Masciovecchio, H. Amenitsch, C. Sissi, A. Paciaroni, Polymorphism of human telomeric quadruplexes with drugs: a multi-technique biophysical study, Phys. Chem. Chem. Phys. 22 (20) (2020) 11583–11592, https://doi.org/10.1039/d0cp01483d.
[43] B. Rossi, C. Bottari, S. Catalini, A. Gessini, F. D'Amico, C. Masciovecchio, Synchrotron based UV Resonant Raman scattering for material science,

Molecular and Laser Spectroscopy, Volume 2 (eds V. P. Gupta, Y. Ozaki), Elsevier (2020), Chapter 13, pages 447-478, http://dx.doi.org/10.1016/B978-0-12-818870-5.00013-7
[44] D. A. Case, T. A. Darden, T. E. Cheatham, C. L. Simmerling, J. Wang, R.E. Duke, P. A. Kollman, (2008) Amber 10 (No. BOOK). University of California
[45] K.G. Sprenger, V.W. Jaeger, J. Pfaendtner, The general AMBER force field (GAFF) can accurately predict thermodynamic and transport properties of many ionic liquids, J. Phys. Chem. B 119 (18) (2015) 5882–5895, https://doi.org/10.1021/acs.jpcb.5b00689.
[46] J. Picálek, B. Minofar, J. Kolafa, P. Jungwirth, Aqueous solutions of ionic liquids: study of the solution/vapor interface using molecular dynamics simulations, Phys. Chem. Chem. Phys. 10 (37) (2008) 5765–5775, https://doi.org/10.1039/B806205F.
[47] W. Jiang, T. Yan, Y. Wang, G.A. Voth, Molecular dynamics simulation of the energetic room-temperature ionic liquid, 1-hydroxyethyl-4-amino-1, 2, 4-triazolium nitrate (HEATN), J. Phys. Chem. B 112 (10) (2008) 3121–3131, https://doi.org/10.1021/jp710653g10.1021/jp710653g.s002.
[48] J.M. Martínez, L. Martínez, Packing optimization for automated generation of complex system's initial configurations for molecular dynamics and docking, J. Comput. Chem. 24 (7) (2003) 819–825, https://doi.org/10.1002/jcc.10216.
[49] L. Martínez, R. Andrade, E.G. Birgin, J.M. Martínez, PACKMOL: A package for building initial configurations for molecular dynamics simulations, J. Comput. Chem. 30 (13) (2009) 2157–2164.
[50] B. Hess, H. Bekker, H.J. Berendsen, J.M. Fraaije, LINCS: a linear constraint solver for molecular simulations, J. Comput. Chem. 18 (12) (1997) 1463–1472, https://doi.org/10.1002/(SICI)1096-987X(199709)18:12<1463::AID-JCC4>3.0.CO;2-H.
[51] T. Darden, D. York, L. Pedersen, Particle mesh Ewald: An N· log (N) method for Ewald sums in large systems, J. Chem. Phys. 98 (12) (1993) 10089–10092, https://doi.org/10.1063/1.464397.
[52] G. Bussi, D. Donadio, M. Parrinello, Canonical sampling through velocity rescaling, J. Chem. Phys. 126 (1) (2007) 014101, https://doi.org/10.1063/1.2408420.
[53] M.J. Abraham, T. Murtola, R. Schulz, S. Páll, J.C. Smith, B. Hess, E. Lindahl, GROMACS: High performance molecular simulations through multi-level parallelism from laptops to supercomputers, SoftwareX 1 (2015) 19–25, https://doi.org/10.1016/j.softx.2015.06.001.
[54] S. Páll, M.J. Abraham, C. Kutzner, B. Hess, E. Lindahl, Tackling exascale software challenges in molecular dynamics simulations with GROMACS, in: In International conference on exascale applications and software, 2014, pp. 3–27, https://doi.org/10.1007/978-3-319-15976-8_1.
[55] S. Pronk, S. Páll, R. Schulz, P. Larsson, P. Bjelkmar, R. Apostolov, M. R. Shirts, J. C. Smith, P. M. Kasson, D. van der Spoel, B. Hess, E. Lindahl, GROMACS 4.5: a high-throughput and highly parallel open source molecular simulation toolkit, Bioinformatics, 29(7) (2013) 845-854 doi: 10.1093/bioinformatics/btt055.
[56] B. Hess, C. Kutzner, D. Van Der Spoel, E. Lindahl, GROMACS 4: algorithms for highly efficient, load-balanced, and scalable molecular simulation, J. Chem. Theory Comput. 4 (3) (2008) 435–447, https://doi.org/10.1021/ct700301q.
[57] D. Van Der Spoel, E. Lindahl, B. Hess, G. Groenhof, A.E. Mark, H.J.C. Berendsen, GROMACS: fast, flexible, and free, J. Comput. Chem. 26 (16) (2005) 1701–1718, https://doi.org/10.1002/jcc.20291.
[58] W. Humphrey, A. Dalke, K. Schulten, VMD: visual molecular dynamics, J. Mol. Graph. 14 (1) (1996) 33–38, https://doi.org/10.1016/0263-7855(96)00018-5.
[59] S. Genheden, A. Reymer, P. Saenz-Méndez, L. A. Eriksson, Computational Chemistry and Molecular Modelling Basics, in *Computational Tools for Chemical Biology* pp. 1-38 (2017) DOI: 10.1039/9781788010139-00001
[60] S.P.A. Fodor, R.P. Rava, T.R. Hays, T.G. Spiro, Ultraviolet resonance Raman spectroscopy of the nucleotides with 266-, 240-, 218-, and 200-nm pulsed laser excitation, J. Am. Chem. Soc. 107 (6) (1985) 1520–1529, https://doi.org/10.1021/ja00292a012.
[61] S.P.A. Fodor, T.G. Spiro, Ultraviolet resonance Raman spectroscopy of DNA with 200–266-nm laser excitation, J. Am. Chem. Soc. 108 (12) (1986) 3198–3205, https://doi.org/10.1021/ja00272a006.
[62] J.G. Duguid, V.A. Bloomfield, J.M. Benevides, G.J. Thomas Jr., Raman Spectroscopy of DNA-Metal Complexes. I. The Thermal Denaturation of DNA in the Presence of Sr', $Ba^{2·}$ $Mg^{2+·}$ $Ca^{2+·}$ $Mn^{2+·}$ $C0^{2+·}$ $Ni^{2+·}$ and Cd^{2+}, Biophys. J. 69 (1995) 2623–2641, https://doi.org/10.1016/S0006-3495(95)80133-5.
[63] P.Y. Turpin, L. Chinsky, A. Laigle, B. Jollès, DNA structure studies by resonance Raman spectroscopy, J. Mol. Struct. 214 (1989) 43–70, https://doi.org/10.1016/0022-2860(89)80005-5.
[64] S.C. Erfurth, W.L. Peticolas, Melting and premelting phenomenon in DNA by laser Raman scattering, Biopolymers 14 (2) (1975) 247–264, https://doi.org/10.1002/bip.1975.360140202.
[65] Z.Q. Wen, G.J. Thomas Jr., UV resonance Raman spectroscopy of DNA and protein constituents of viruses: assignments and cross sections for excitations at 257, 244, 238, and 229 nm, Biopolymers 45 (5) (1998) 247–256, https://doi.org/10.1002/(SICI)1097-0282(199803)45:3<247::AID-BIP7>3.0.CO;2-R.
[66] J.G. Duguid, V.A. Bloomfield, J.M. Benevides, G.J. Thomas, DNA melting investigated by differential scanning calorimetry and Raman spectroscopy, Biophys. J. 71 (6) (1996) 3350–3360, https://doi.org/10.1016/S0006-3495(96)79528-0.
[67] S.S. Chan, R.H. Austin, I. Mukerji, T.G. Spiro, Temperature-Dependent Ultraviolet Resonance Raman Spectroscopy of the Premelting State of dA* dT DNA, Biophys. J. 72 (4) (1997) 1512–1520, https://doi.org/10.1016/S0006-3495(97)78799-X.
[68] B.L. Tomlinson, W.L. Peticolas, Conformational Dependence of Raman Scattering Intensities in Polyadenylic Acid, J. Chem. Phys. 52 (4) (1970) 2154–2156, https://doi.org/10.1063/1.1673270.
[69] L. Movileanu, J.M. Benevides, G.J. Thomas Jr, Temperature Dependence of the Raman Spectrum of DNA. Part I—Raman Signatures of Premelting and Melting Transitions of Poly(dA–dT)·Poly(dA–dT), J. Raman Spectrosc. 30 (1999) 637–649, https://doi.org/10.1002/(SICI)1097-4555(199908)30:8<637::AID-JRS431>3.0.CO;2-B.
[70] I. Mukerji, A.P. Williams, UV resonance Raman and circular dichroism studies of a DNA duplex containing an A(3)T(3) tract: evidence for a premelting transition and three-centered H-bonds, Biochemistry 41 (2002) 69–77, https://doi.org/10.1021/bi010918i.
[71] L. Chinsky, P.Y. Turpin, Ultraviolet resonance Raman study of DNA and of its interaction with actinomycin D, Nucleic Acid Res. 5 (8) (1978) 2969–2978, https://doi.org/10.1093/nar/5.8.2969.
[72] L. Movileanu, J.M. Benevides, G.J. Thomas Jr, Determination of base and backbone contributions to the thermodynamics of premelting and melting transitions in B DNA, Nucleic Acids Res. 30 (17) (2002) 3767–3777, https://doi.org/10.1093/nar/gkf471.
[73] L.A. Marky, K.J. Breslauer, Calculating thermodynamic data for transitions of any molecularity from equilibrium melting curves, Biopolymers 26 (9) (1987) 1601–1620.
[74] J.D. Puglisi, I. Tinoco Jr., [22] absorbance melting curves of RNA, Methods Enzymol. 180 (1989) 304–325, https://doi.org/10.1016/0076-6879(89)80108-9.
[75] K. Shimizu, M. Tariq, M.F.C. Gomes, L.P.N. Rebelo, J.N.C. Lopes, Assessing the dispersive and electrostatic components of the cohesive energy of ionic liquids using molecular dynamics simulations and molar refraction data, J. Phys. Chem. B 114 (17) (2010) 5831–5834, https://doi.org/10.1021/jp101910c.
[76] L. Santos, J.N.C. Lopes, J.A.P. Coutinho, J. Esperanca, L.R. Gomes, I.M. Marrucho, L.N. Rebelo, Ionic liquids: first direct determination of their cohesive energy, J. Am. Chem. Soc. 129 (2007) 284–285, https://doi.org/10.1021/ja067427b.
[77] T. Köddermann, D. Paschek, R. Ludwig, Molecular dynamic simulations of ionic liquids: a reliable description of structure, thermodynamics and dynamics, Chem. Phys. Chem. 8 (17) (2007) 2464–2470, https://doi.org/10.1002/cphc.200700552.
[78] L. Rimai, V.M. Maher, D. Gill, I. Salmeen, J.J. McCormick, The temperature dependence of Raman intensities of DNA. Evidence for premelting changes and correlations with ultraviolet spectra, Biochim. Biophys. Acta 361 (2) (1974) 155–165, https://doi.org/10.1016/0005-2787(74)90343-8.
[79] J.M. Benevides, S.A. Overman, G.J. Thomas, Raman, polarized Raman and ultraviolet resonance Raman spectroscopy of nucleic acids and their Complexes, J. Raman Spectrosc. 36 (4) (2005) 279–299, https://doi.org/10.1002/jrs.1324.
[80] N. Fujimoto, A. Toyama, H. Takeuchi, Effects of hydrogen bonding on the UV resonance Raman bands of the adenine ring and its C8-deuterated analog, J. Mol. Struct. 447 (1-2) (1998) 61–69, https://doi.org/10.1016/S0022-2860(98)00301-9.
[81] A. Toyama, H. Takeuchi, I. Harada, Ultraviolet resonance Raman spectra of adenine, uracil and thymine derivatives in several solvents. Correlation between band frequencies and hydrogen-bonding states of the nucleic acid bases, J. Mol. Struct. 242 (1991) 87–98, https://doi.org/10.1016/0022-2860(91)87129-6.
[82] M. Tsuboi, M. Komatsu, J. Hoshi, E. Kawashima, T. Sekine, Y. Ishido, M.P. Russell, J.M. Benevides, G.J. Thomas, Raman and infrared spectra of (2'S)-[2'-2H]Thymidine: vibrational coupling between deoxyribosyl and thymine moieties and structural implications, J. Am. Chem. Soc. 119 (1997) 2025–2032, https://doi.org/10.1021/ja962676t.
[83] A. Jirasek, H.G. Schulze, C.H. Hughesman, A.L. Creagh, C.A. Haynes, M.W. Blades, R.F.B. Turner, Discrimination between UV radiation-induced and thermally induced spectral changes in AT-paired DNA oligomers using UV resonance Raman spectroscopy, J. Raman Spectrosc. 37 (12) (2006) 1368–1380, https://doi.org/10.1002/jrs.1552.
[84] N.V. Hud, V. Sklenar, J. Feigon, Localization of ammonium ions in the minor groove of DNA duplexes in solution and the origin of DNA A-tract bending, J. Mol. Biol. 286 (1999) 651–660, https://doi.org/10.1006/jmbi.1998.2513.
[85] N.V. Hud, J. Feigon, Localization of divalent metal ions in the minor groove of DNA A-tracts, J. Am. Chem. Soc. 119 (24) (1997) 5756–5757, https://doi.org/10.1021/ja9704085.
[86] G.S. Manning, The molecular theory of polyelectrolyte solutions with applications to the electrostatic properties of polynucleotides, Q. Rev. Biophys. 11 (2) (1978) 179–246, https://doi.org/10.1017/s0033583500002031.
[87] M.A. Young, B. Jayaram, D.L. Beveridge, Intrusion of counterions into the spine of hydration in the minor groove of B-DNA: fractional occupancy of electronegative pockets, J. Am. Chem. Soc. 119 (1) (1997) 59–69, https://doi.org/10.1021/ja960459m.
[88] S.Y. Ponomarev, K.M. Thayer, D.L. Beveridge, Ion motions in molecular dynamics simulations on DNA, Proc. Natl. Acad. Sci. U.S.A. 101 (41) (2004) 14771–14775, https://doi.org/10.1073/pnas.0406435101.